CHAPTER III

RESULTS AND DISCUSSION

CEC

1. Single Exchangeable Cations

The cation exchange capacities of Bang Rin kaolinite, bentonite and marl with various cations are tabulated in Table 3.1. The results are given in millimoles (mmol) of each cation per 100 g of the dry weight. The CEC decreases in the order:

Bentonite > Kaolinite > Marl

except for calcium ion exchange capacity. The calcium ion exchange capacity in marl is markedly higher than the values for bentonite and kaolinite. The exchange capacity for ferric ion is small in comparison with values for the other ions.

From Table 3.1 the CEC of bentonite decreases in the order:

$$Ca^{2+} > Na^{+} > Fe^{2+} > K^{+} > Zn^{2+} > Fe^{3+}$$

In kaolinite the CEC decreases in the order:

$$Fe^{2+} > K^{+} > Ca^{2+} > Na^{+} > Zn^{2+} > Fe^{3+}$$

In marl the CEC decreases in the order:

$$Ca^{2+} > Zn^{2+} > K^{+} > Fe^{3+}, Fe^{2+}$$

The orders of CEC in these materials are all different.

The relevant ionic radii are shown in Table 3.2, which decrease in order:

$$K^{+} > Ca^{2+} > Na^{+} > Fe^{2+} > Zn^{2+} > Fe^{3+}$$

Table 3.1 The CEC's of bentonite, kaolinite and marl

Type of clay minerals \ Adsorbed cations (mmol/100 g)	Fe^{3+}	Fe^{2+}	Zn^{2+}	Ca^{2+}	Na^{+}	K^{+}
Bentonite	6.76(±1.0)	35.42(±0.3)	23,40(±1,0)	53.23(±3.0)	39.01(±0.4)	32.25(±1.0)
Kaolinite	1.53(±0.2)	14.03(±2.0)	5.74(±2.0)	10.15(±2.0)	8.85(±0.5)	10.31(±0.5)
Marl	0.00	0.00	4.31(±0.2)	86.03(±6.0)	3.01(±0.1)	3.95(±0.4)

Table 3.2 Ionic Radii of some cations.

Element	Atomic Number	Ionic Radius in Å
Na	11	(+1) 0.95
K	19	(+1) 1.33
Ca	20	(+2) 0.99
Fe	26	(+2) 0.75
		(+3) 0.64
Zn	30	(+2) 0.74

In aqueous solution, this order is reversed. Small ions bind more water than larger ions, so the sizes of the hydrated cations decrease in the order:

$$Fe^{3+} > Zn^{2+} > Fe^{3+} > Na^{+} > Ca^{2+} > K^{+}$$

If the CEC increased as the particle size decreased, the order of CEC would be:

$$K^{+} > Ca^{2+} > Na^{+} > Fe^{2+} > Zn^{2+} > Fe^{3+}$$

As shown in Table 3.1 the CEC of Kaolinite seem to follow this order, with the exception of Fe^{2+}.

For the ferric ion, the smallness of CEC may be due to the low pH of $FeCl_3$ solution as shown in Table 3.3. At low pH's the exchange capacity of the clay may be reduced either by destruction of its structure through acid attack or by clogging of the exchange position by migrating octahedral aluminum ions (44). Low CEC values were therefore expected. Also, assuming that the negative charge in the clay structure arises primarily from isomorphous substitution (45) and broken bonds at the crystal edges (46), a reduction in pH would cause neutralization of the edge charges by protons and consequently lower the CEC.

From previous work (55) on the iron binding capacity of marl, determined by radio iron and chemical iron techniques, it was shown that 1 mg of marl could bind iron up to 37 μg and it was concluded that marl may be used for the prevention of iron overload from dietary iron.

In this study, it was found that saturation of marl with Fe^{3+} ions did not result in a simple exchange reaction. It was observed that a considerable amount of gas evolved from the reaction mixture.

Table 3.3 pH of some inorganic salt solutions.

Solution	pH
NaCl	7
KCl	7
$FeCl_3.6H_2O$	1.5
$CaCl_2$	4.5
$Zn(NO_3)2.6H_2O$	3
$FeSO_4.7H_2O$	3.5

Since marl is mainly carbonates of magnesium and calcium this gas was presumably carbon dioxide. Occurrence of reactions other than a cation exchange implies that Fe^{3+} could end up as an oxide or carbonate in the solid phase, and not as an 'exchangeable' ion. Consequently, washing the 'Fe^{3+}-exchanged' marl with a solution of NH_4^+ amounted to no displacement of Fe^{3+} by NH_4^+ and resulted in zero exchange capacity.

The solid product of the reaction between marl and the Fe^{3+} solution was red-brown in color. Attempt to identify this by X-ray analysis was unsuccessful probably because the particle size was too small to give X-ray diffraction peaks.

2. Mixed Exchangeable Cation

The mixed-cation exchange capacities of Bang Rin kaolinite, bentonite and marl are tabulated in Table 3.4, 3.5 and 3.6 respectively.

Data tabulated in Tables 3.4-3.6 indicate that in general the values of individual mixed CEC's are higher than those of the coores-ponding single CEC. This is true for Zn^{2+}, Ca^{2+}, Na^{+} and K^{+} on kaolinite. In these cases, the total mixed CEC's are of the same order of magnitude as the sum of the single CEC's, suggesting that similar exchange sites are involved in single-ion and mixed-ion exchange reactions and probably that different cations occupy different sites, Exceptions occur with Zn^{2+} and Ca^{2+} for which mixed CEC's are somewhat higher than the corresponding single CEC. Apparently certain combinations of cations somehow have the effect of exposing new exchange sites on the surfaces of the clays. Also, solution pH affects the CEC's of clays (9) to some extent but the effect of pH in the present work cannot be estimated since all saturated solu-tions were unbuffered.

The "CEC's" for marl show some peculiarities. In all cases, except for Na^{+}, the single CEC values are always higher than the corres-ponding mixed CEC values. Again, it should be emphasized that the reaction involved are by no mean simple exchange reactions and it is doubtful whether CEC values reported for marl in this work or elsewhere (55) can be accepted as such. Nevertheless, it can be seen that marl has a high affinity for Ca^{2+} and none for exchangeable Fe^{3+} and Fe^{2+}. On the other hand, the result for Ca^{2+} may be viewed in terms of the nature of marl as compared to kaoli-nite and bentonite. Marl consists largely of calcium carbonate and probably of other calcium salts. The extremely high value for "exchangeable" Ca^{2+} probable suggests that the excess Ca^{2+} ions could not be completely removed by five washings (with ammonium nitrate solution) and/or that additional Ca^{2+} ions are somehow released during the saturation and washing processes.

Table 3.4 Comparison between mixed CEC and single CEC of Kaolinite

Exchanging Cation	CEC (mmol/100 g)*								
	Single	Mixed							
Fe^{3+}	1.53								
Fe^{2+}	14.03	12.65(±2.0)			7.74(±1.0)				
Zn^{2+}	5.74	10.21(±0.1)	7.17(±1.0)	7.73(±0.1)				5.31(±0.3)	
Ca^{2+}	10.15			15.36(±0.1)		19.45(±0.2)			15.79(±0.1)
Na^{+}	8.85		8.97(±1.0)		11.47(±0.5)	11.47(±1.0)	4.01(±0.4)		
K^{+}	10.31						5.40(±1.0)	6.33(±0.1)	10.92(±0.1)
Total	-	22.86	16.14	23.09	19.48	30.92	9.41	11.64	26.71

* each CEC value is an average from three determinations the spread of which is indicated in parenthesis.

Table 3.5 Comparison between mixed CEC and single CEC of Bentonite.

Exchanging Cations	CEC (mmol/100 g)*								
	Single	Mixed							
Fe^{3+}	6.76								
Fe^{2+}	35.42	10.04(±0.2)			21.30(±1.0)				
Zn^{2+}	23.40	10.85(±1.0)	19.61(±2.0)	12.45(±2.0)				21.61(±0.1)	
Ca^{2+}	53.23			38.45(±2.0)		57.23(±3.0)			36.89(±0.6)
Na^{+}	39.01		8.13(±1.0)		15.62(±1.0)	14.71(±2.0)	10.96(±0.2)		
K^{+}	32.25						29.71(±0.5)	8.97(±0.3)	18.65(±0.3)
Total	-	20.89	27.74	50.90	36.92	71.94	40.67	30.58	55.54

* each CEC value is an average from three determinations the spread of which is indicated in parenthesis.

Table 3.6 Comparison between mixed CEC and single CEC of Marl.

Exchanging Cation	CEC (mmol/100 g)*								
	Single	Mixed							
Fe^{3+}	0.00								
Fe^{2+}	0.00	0.00			0.00				
Zn^{2+}	4.31	1.42(±0.1)	4.25(±0.1)	2.95(±0.1)				4.82(±0.4)	
Ca^{2+}	86.03			60.83(±0.4)		63.69(±0.3)			29.46(±0.1)
Na^{+}	3.01		1.38(±0.1)		0.66(±0.1)	1.93(±0.3)	5.79(±1.0)		
K^{+}	3.95						1.24(±0.4)	0.02(±0.1)	0.43(±0.2)
Total	-	1.42	5.63	63.78	0.66	65.62	7.03	4.48	29.89

* each CEC value is an average from three determinations the spread of which is indicated in parenthesis.

Intercalation Complexes

1. X-ray Diffraction Study

1.1 Intercalation of Organic Reagents into Marl, Kaolinite and Bentonite

Table 3.7 summarizes results from exposure of the clay to a number of organic reagents for 1 hour. All organic reagents were capable of forming intercalation complexes with kaolinite, but could not complex with marl or bentonite. Complex formation was accompanied by an increase in the d(001) spacing from 7.19 Å for kaolinite to a higher value. Complete complex formation was indicated by disappearance of the 7.196 Å diffraction peak and the appearance of the new d(001) peak at a lower angle (larger spacing). Comparison of x-ray diffraction patterns in Figure 3.1 and 3.2 showed that the interlayer spacing of the complexes decreased in the order:

DMSO > DMF > paraquat

Intercalation of DMF and DMSO into kaolinite occurred to a small extent after 1 hour. The x-ray diffraction pattern of paraquat-kaolinite complex after 1 hour showed that only a small proportion of kaolinite was expanded. The extent of intercalation gradually increased as the exposure time increased. However, complete complex formation was not observed.

All these organic reagents have functional groups which are able to from hydrogen bonds with kaolinite, such as the carbonyl and the amine group. However, formation of the complexes is strongly dependent on the properties of the organic compound, and generally a large dipole moment favours the formation of a complex (7).

Table 3.7 - Complex Formation of Bang Rin Kaolin with organic Reagents

Reagents	Interlayer spacing, Å Bang Rin
Untreated Kaolinite	7.196
DMSO (Dimethyl Sulphoxide)	9.825
DMF (Dimethyl formamide)	8.346
paraquat	8.043

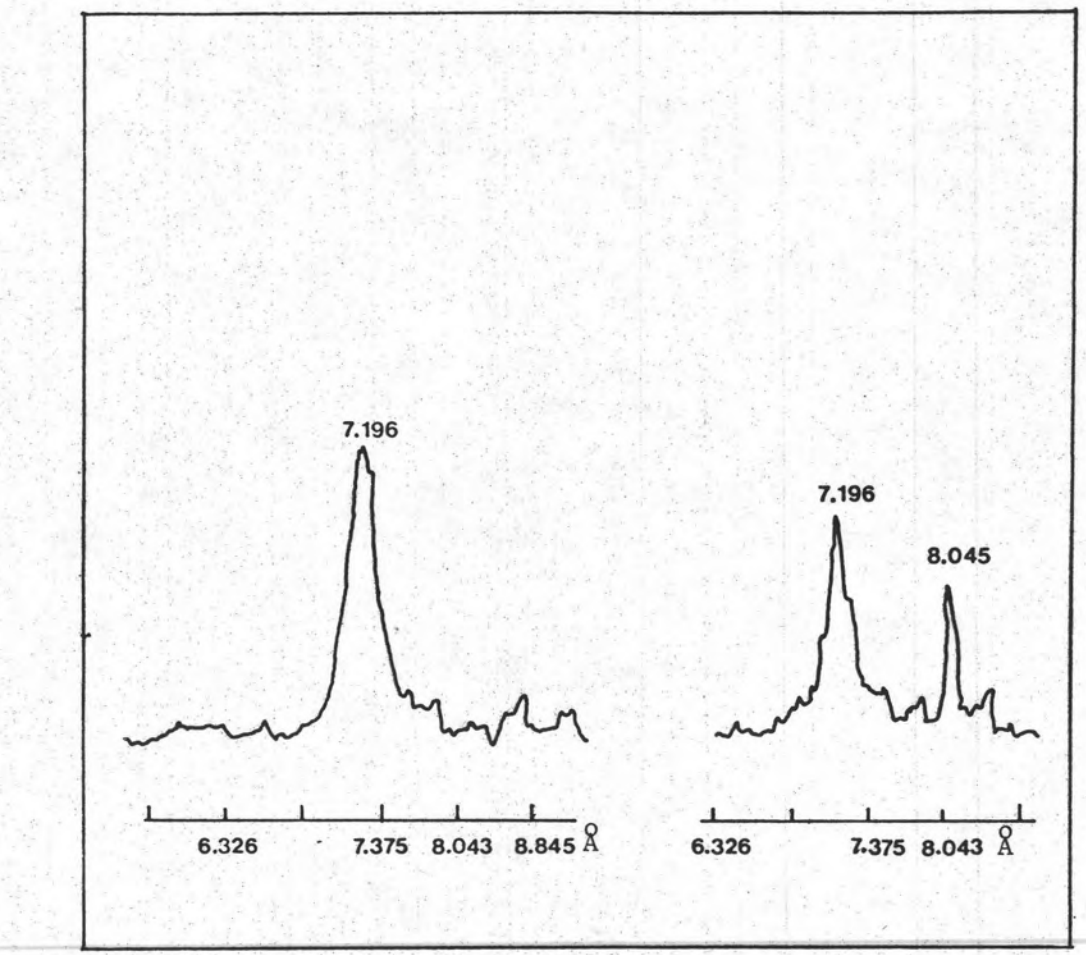

Figure 3.1 X-ray diffraction patterns of 1 hour treatment of

(a) Untreated kaolinite

(b) Paraquat-kaolinite complex

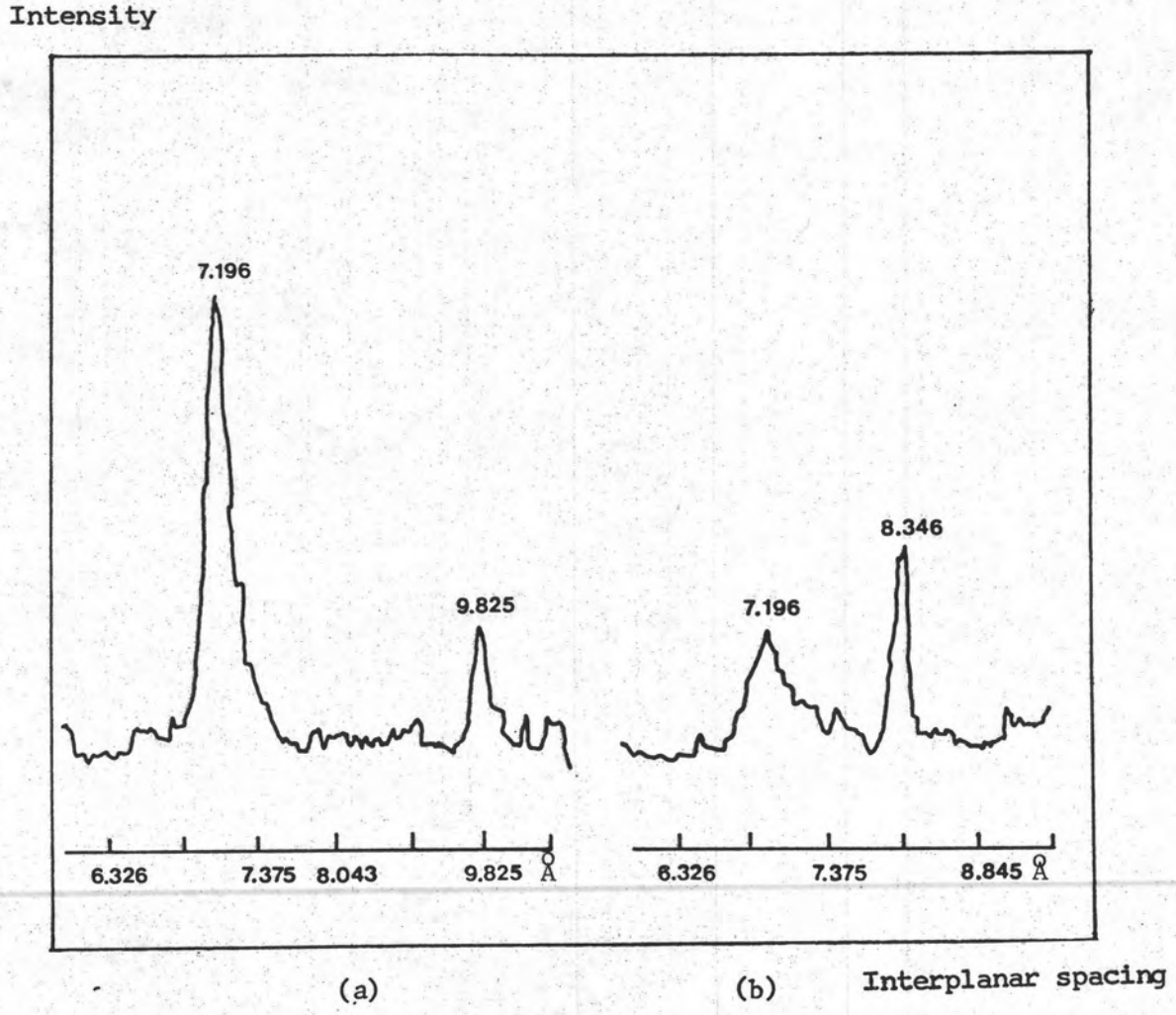

Fiqure 3.2 X-ray diffraction pattern of 1 hour treatment of

(a) DMSO-kaolinite complex

(b) DMF-kaolinite complex

The dipole moments of DMSO and DMF are 4.3 and 3.82 debye respectively (7). The dipole moment of paraquat has not been reported, but bipyridine which has a similar structure has a dipole moment of 1.7 debye (7). Comparison between the dipole moment of DMF and DMSO shows that DMSO is more polar, and causes a larger expansion in kaolinite layer than DMF does. The dipole moment of paraquat is believed to be smaller than those of DMF and DMSO and paraquat should cause a smaller expansion in kaolinite layer compared with DMF and DMSO.

From previous work (13) bentonite was used to prevent the absorption of paraquat into the plasma and accumulation of paraquat in the lung of rats. This treatment consists of a stomach wash followed by four administrations of plus purgatives at two-to three-hour intervals. Even when treatment was delayed until 10 hours after administration of paraquat 80 % survival was obtained.

In this study it was found that bentonite has a higher CEC than kaolinite and marl in both single and mixed ion methods. From x-ray diffraction analysis it was found that paraquat cannot intercalate into bentonite since no new x-ray peaks were obscured. It is suggested, therefore, that paraquat was adsorbed only on the surface of bentonite. Also, in view of the fact that an intercalated complex can be formed between kaolinite and paraquat, it is possible that kaolinite can act as an immediate antidote to paraquat poisoning.

1.2 Intercalation of Inorganic Salts into Kaolinite, Bentonite and Marl

In most cases, 1 mol/dm^3 salt solutions were used. Preparation of the intercalation complexes was done at room temperature. Only CH_3COOK can intercalate into kaolinite as shown in Figure 3.3. For marl and bentonite none of the salts was capable of forming an intercalation complex.

In the case of CH_3COOK, examination of the X-ray diffraction pattern shows that after 1 hour the clay was expanded to 14 Å.

Weiss et al. (20) suggest that intercalation is a function of cation radius. They also suggest a mechanism for the intercalation reaction which stresses the role of hydrogen bonding. The lone-pair electron of the carbonyl oxygen in the acetate ion are more available for hydrogen bonding than those of the siloxane groups of kaolinite.

Wada (1) suggests that the intercalation contains a monomolecular layer of water along with the acetate. Wada's concept of the arrangement of the intercalated acetate is shown in Figure. 3.4

Garrett and Walker (56) found that a high salt concentration is necessary before significant intercalation occurs.

This suggestion is apparently supported by the intercalation of CH_3COOK into kaolinite and also implies that the concentration of inorganic salt solutions used in this experiment may be too low to cause intercalation in kaolinite.

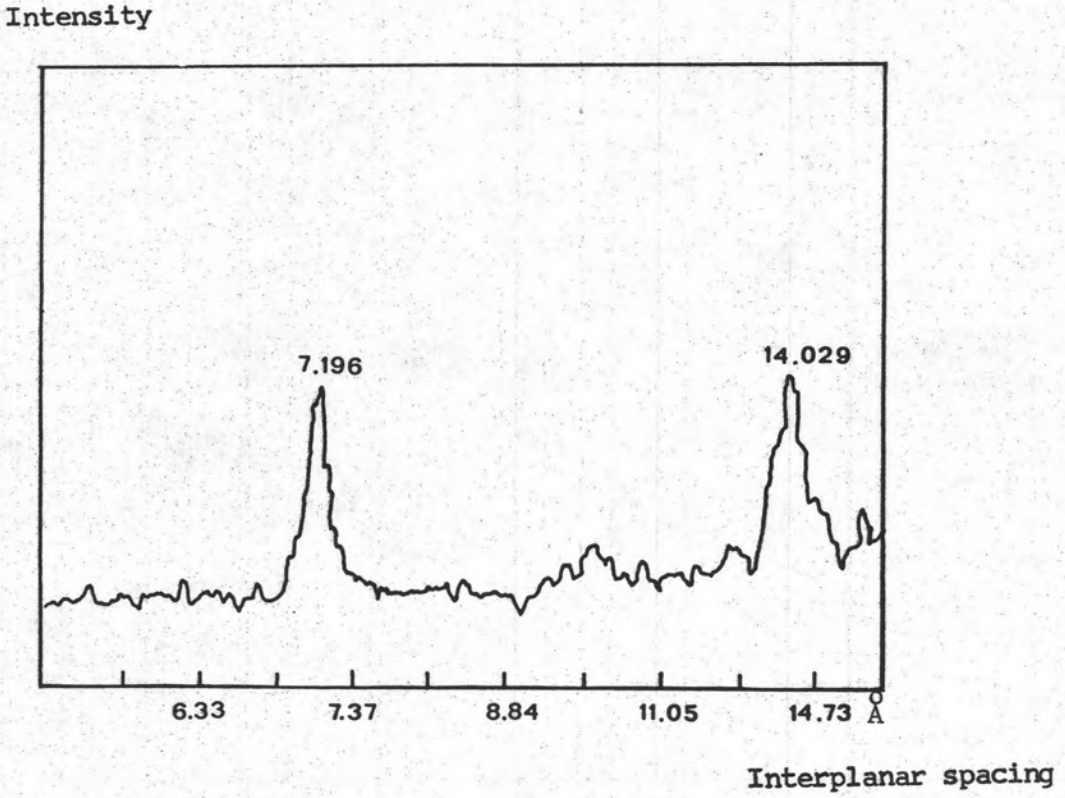

Figure 3.3 X-ray diffraction pattern (1-hour exposure) of CH_3COOK-kaolinite complex.

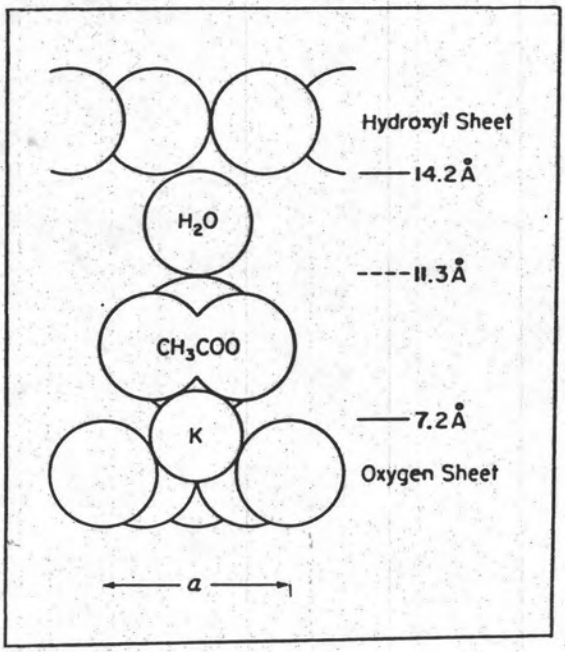

Figure 3.4 A cross section of the 14 Å complex, showing a probable position of K^+, $C_2H_3O_2^-$, and H_2O.

2. IR Study

2.1 "Bang Rin" Kaolinite

IR spectra of Kaolinite ("Bang Rin") in the hydroxyl absorption region are shown in Figure 3.5. There are seven absorption peaks at 3680, 3670, 3660, 3650, 3640, 3630, and 3610 cm^{-1}, and a broad band at approximately 3400 cm^{-1}. Only two of these (at 3680 and 3610 cm^{-1}) are prominent absorption peaks. The peaks at 3670, 3660, and 3630 cm^{-1} appear as shoulders.

Previous attempts to correlate these ν(OH) stretching frequencies of kaolinite to corresponding OH lattice sites were based entirely on the ideal structural model. Nowadays the assignments of the hydroxyl absorption bands to definite positions in the crystal lattice of kaolinite are essentially based on the hydrogen bonding interaction between the lattice OH ions and the structural groups of intercalated and on OH-OD shifts produced by selective deuteration.

There have been several attempts to associate absorption bands appearing in the OH stretching region (3750 to 3000 cm^{-1}) with structural OH groups in the lattice of kaolinite.

The structure of kaolinite is represented by the (100) projection shown in Figure 3.6.

Serratosa, Hildago, and Vinas (8) found that kaolinite shows four absorption bands at 3695, 3670, 3650, and 3620 cm^{-1}. The band at 3695 cm^{-1} corresponds to OH bonds in a direction nearly normal to the flakes. These OH's must be almost free, that is, not participating in any significant hydrogen bonding association. The 3620 cm^{-1} band must be assigned to OH directed to the unoccupied octrahedra. The other obsorptions at 3670 and 3650 cm^{-1} must correspond to OH which are participating in hydrogen bonding between layers. The existence of the

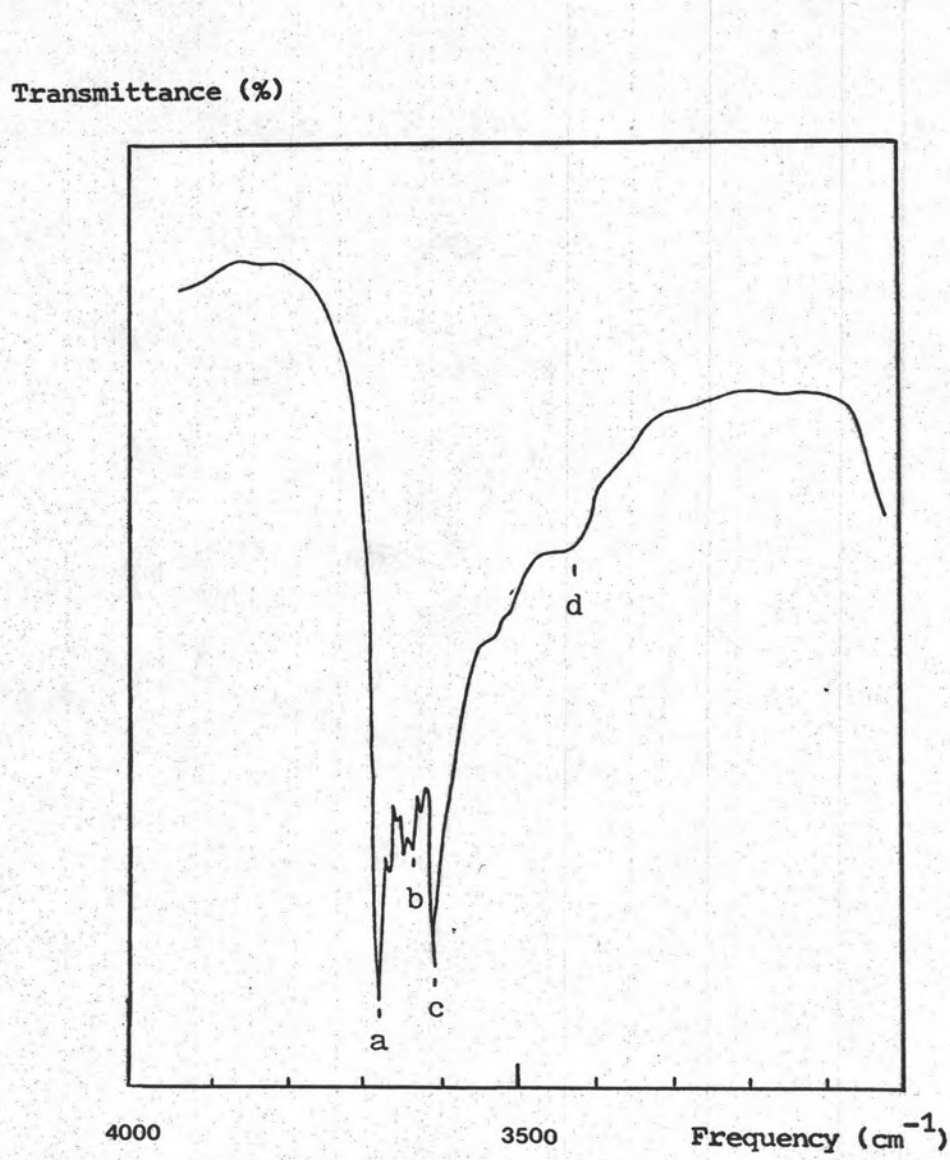

Figure 3.5 OH stretching bands of "Bang Rin" kaolinite

Maximum absorptions are situated at:

(a) 3680 cm^{-1};

(b) 3640 cm^{-1};

(c) 3610 cm^{-1};

(d) ~3400 cm^{-1}.

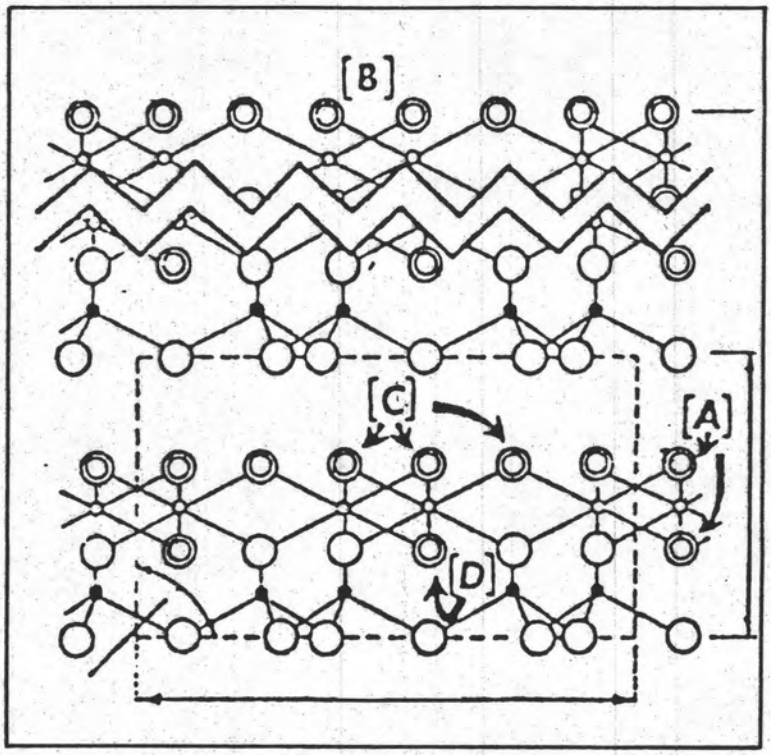

Figure 3.6 Projection of the structure of kaolinite on the (100) plane showing the stacking of successive layers in a micro crystal. A and B indicate "outer hydroxyls"; C designates "inner-surface hydroxyls"; D indicates "inner-hydroxyls".

two weak aborptions presumably indicates that the weak bonds are of two different kinds. Wolff (58) observed that kaolinite had three absorption bands at 3704, 3663, and 3635 cm^{-1}. His assignments were essentially identical to those proposed by Serratosa, Hidalgo, and Vinas with the exception that OH groups located at the edges and in fractures of plates would contribute to the intensity of the high freguency absorption band at 3704 cm^{-1}.

Comparison of the present results with those of Serratosa et al. suggests that the "extra" peaks and shoulders may be due to a higher structural disorder arising from randomness in the stacking of successive layers in the c-direction in "Bang Rin" kaolinite. The broad band at approximately 3400 cm^{-1} is believed to be due to vibrations of OH bonds of externally adsorbed water (59).

2.2 Intercalation of Organic Reagents into kaolinite

The IR spectra of organic-kaolinite complexes are shown in Figures 3.7 to 3.9.

The infrared spectrum of the DMSO-kaolinite complex after 1-hour contact is shown in Figure 3.7. Sharp absorption bands appear at 3650, 3530, and 3490 cm^{-1}. It has been found (57) that the intensity of these peaks increase with time while that of the 3680 cm^{-1} peak dereased. However, the weak absorptions at 3660, 3640, and 3620 cm^{-1} still appeared in all spectra of the complexes. There are no absorptions at 3670 and 3630 cm^{-1}.

The infrared spectrum of the DMF-kaolinite complexes is shown in Figure 3.8. The absorptions at 3670, 3660 and 3640 cm^{-1} disappeared from the spectrum. The absorptions at 3680, 3650, 3630, 3610, and the broad band at approximately 3400 cm^{-1} are almost the same as those in the kaolinite spectrum.

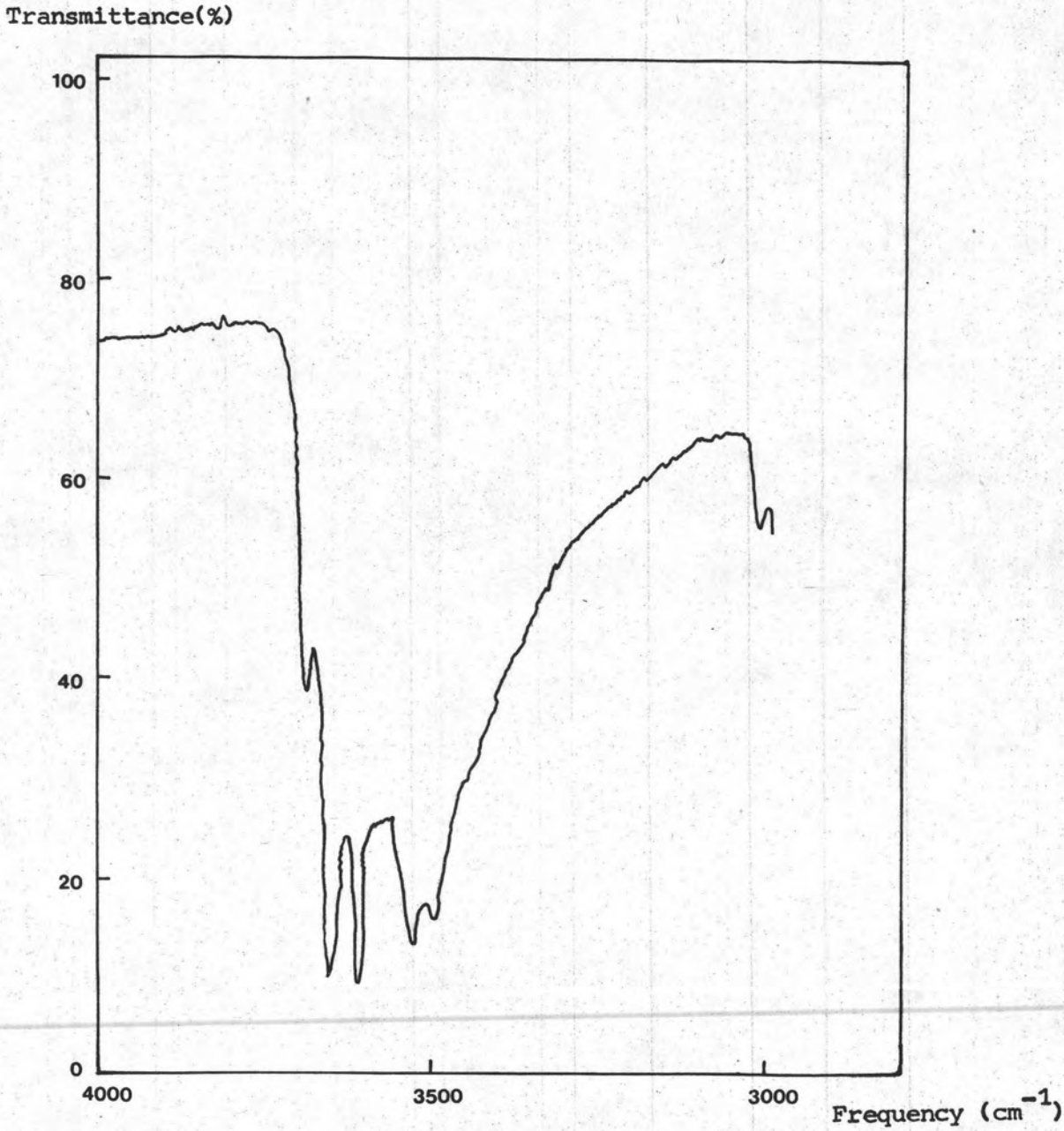

Figure 3.7 OH stretching bands of DMSO-kaolinite complex:

Maximum absorptions are situated at:

(a) 3680 cm^{-1};

(b) 3650 cm^{-1};

(c) 3610 cm^{-1};

(d) 3530 cm^{-1};

(e) 3490 cm^{-1}.

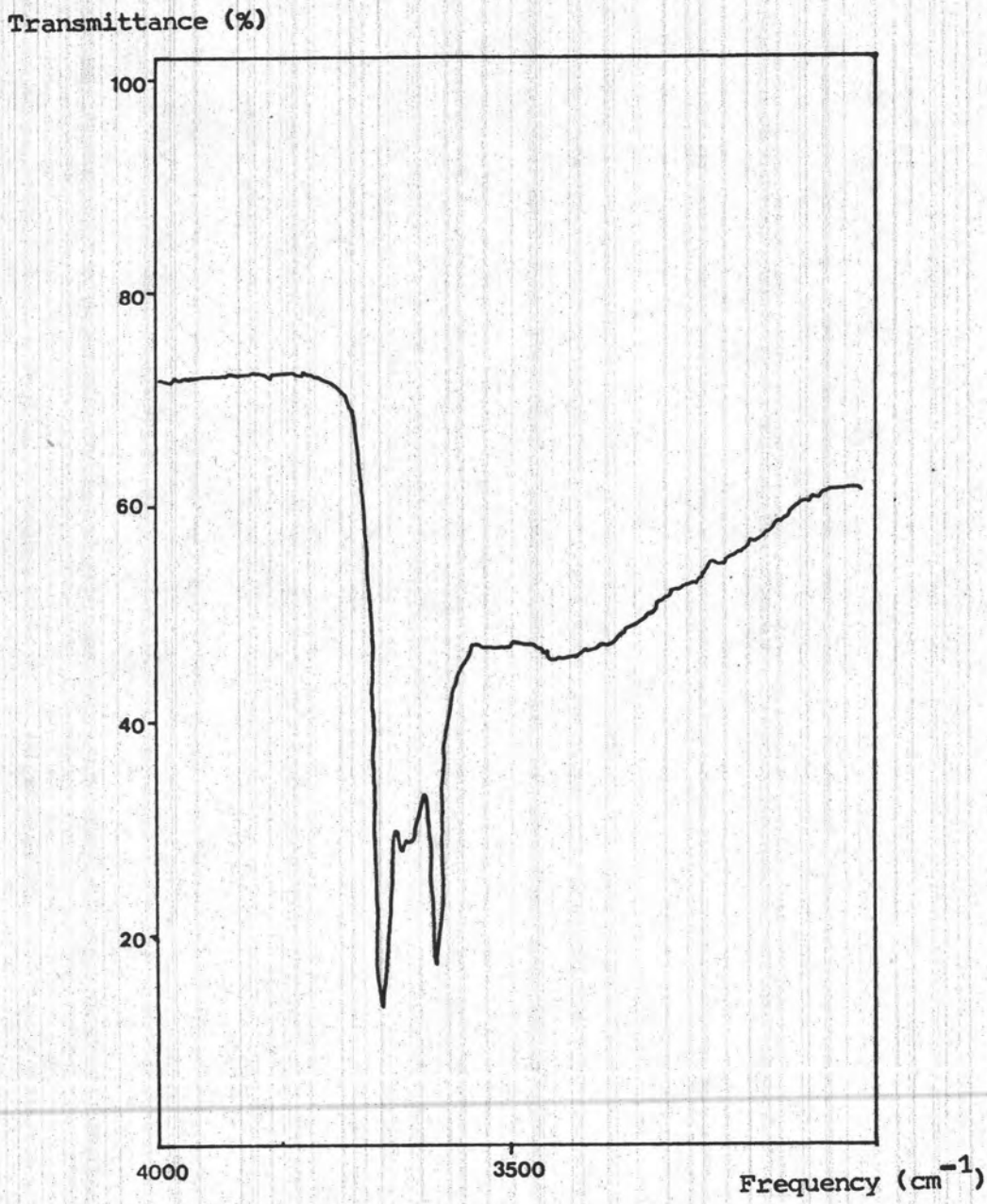

Figure 3.8 OH stretching bands of DMF-kaolinite complex:

Maximum absorptions are situated at:

(a) 3680 cm^{-1};

(b) 3650 cm^{-1};

(c) 3630 cm^{-1};

(d) 3610 cm^{-1};

(e) ~3400 cm^{-1};

The infrared spectrum of the paraquat-kaolinite is shown in Figure 3.9. The spectrum is similar to that of DMF-kaolinite. The absorptions at 3670, 3660, and 3640 cm^{-1} disappeared from the spectrum and a broad band appeared at about 3350 cm^{-1}. The absorption bands at 3680, 3650, 3630 and 3610 cm^{-1} are almost the same as those in the kaolinite spectrum.

The interesting feature in the IR spectrum of the DMSO complex is the appearance of sharp peaks at 3650, 3530, and 3490 cm^{-1} and the decrease in intensity of the peak at 3680 cm^{-1}. The interaction between the oxygen of DMSO and the OH groups of the clay probably gives rise to the new absorption bands at 3530 and 3490 cm^{-1}. Olejnik et al. (22) suggested that crystal field effects and the geometry of the system cause a splitting of the bands. DMSO will arrange itself to give minimum interaction between adjacent molecules (57). This may lead to some of the oxygen atoms of DMSO being similarly positioned with respect to the hydroxyl layer as the oxygen atoms of the adjacent tetrahedral layer in unexpanded kaolinite. The increase in the number of weak hydrogen bonds between these oxygen atoms of DMSO and OH groups of the inner surface of the clay should then result in the increased intensity of the 3650 cm^{-1} bond.

The structure of DMF is as follows:

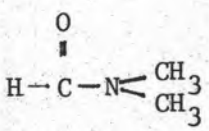

Intercalation occurs with the formation of the hydrogen bond between the oxygen of the CO group and the hydrogen of the inner surface OH. However, there is no new significant absorption band in the IR spectra of the DMF-kaolinite complex.

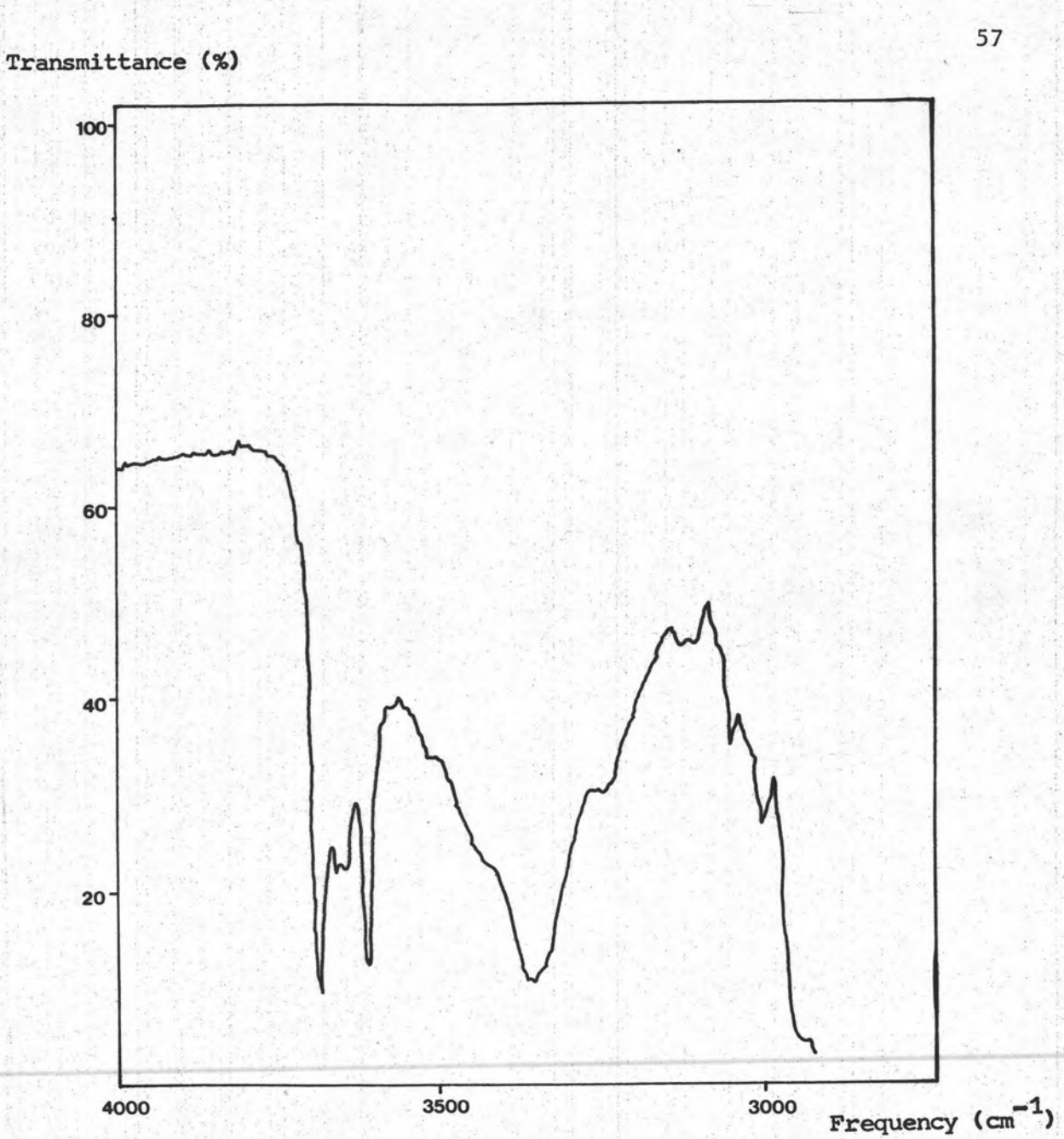

Figure 3.9 OH stretching bands of paraquat-kaolinite complex:

Maximum absorptions are situated at:

(a) 3680 cm^{-1};

(b) 3650 cm^{-1};

(c) 3630 cm^{-1};

(d) 3610 cm^{-1};

(e) 3350 cm^{-1};

The structure of paraquat is as follows:

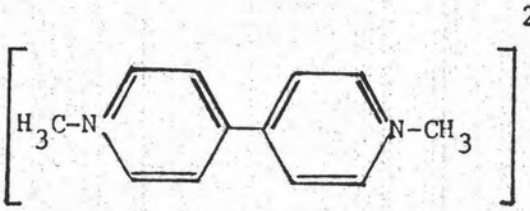

The occurrence of intercalation may be due to the formation of hydrogen bonds between the nitrogen atom in the molecule of paraquat and the OH groups in the inner surface of kaolinite. However, there is no new significant absorption band in the IR spectra of the paraquat-kaolinite complex. The broad band at 3350 cm^{-1} is due to the absorption band of pure paraquat as shown Figure 3.10 and 3.11.

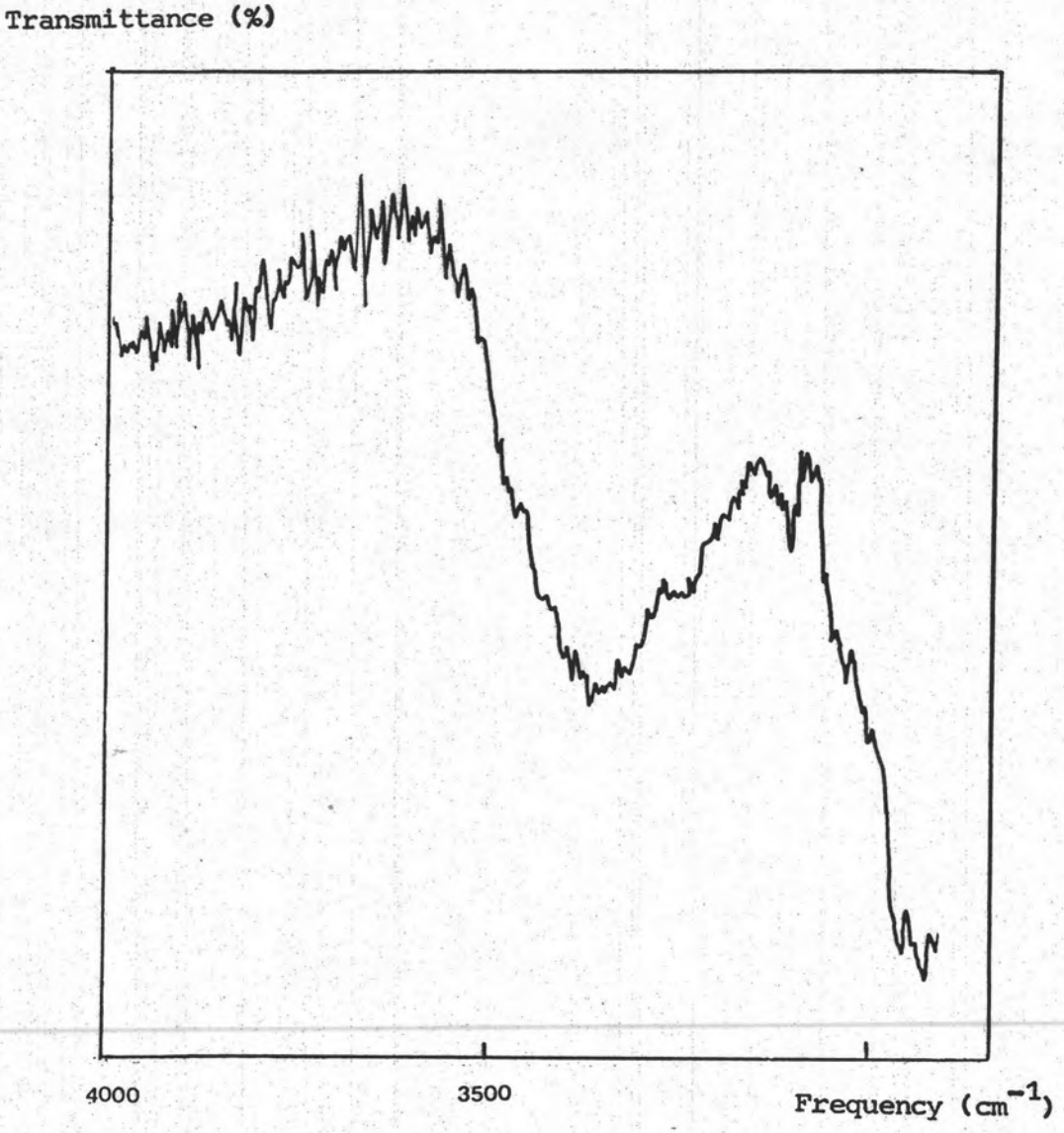

Figure 3.10 Infrared spectrum of paraquat from 2900 to 4000 cm^{-1}

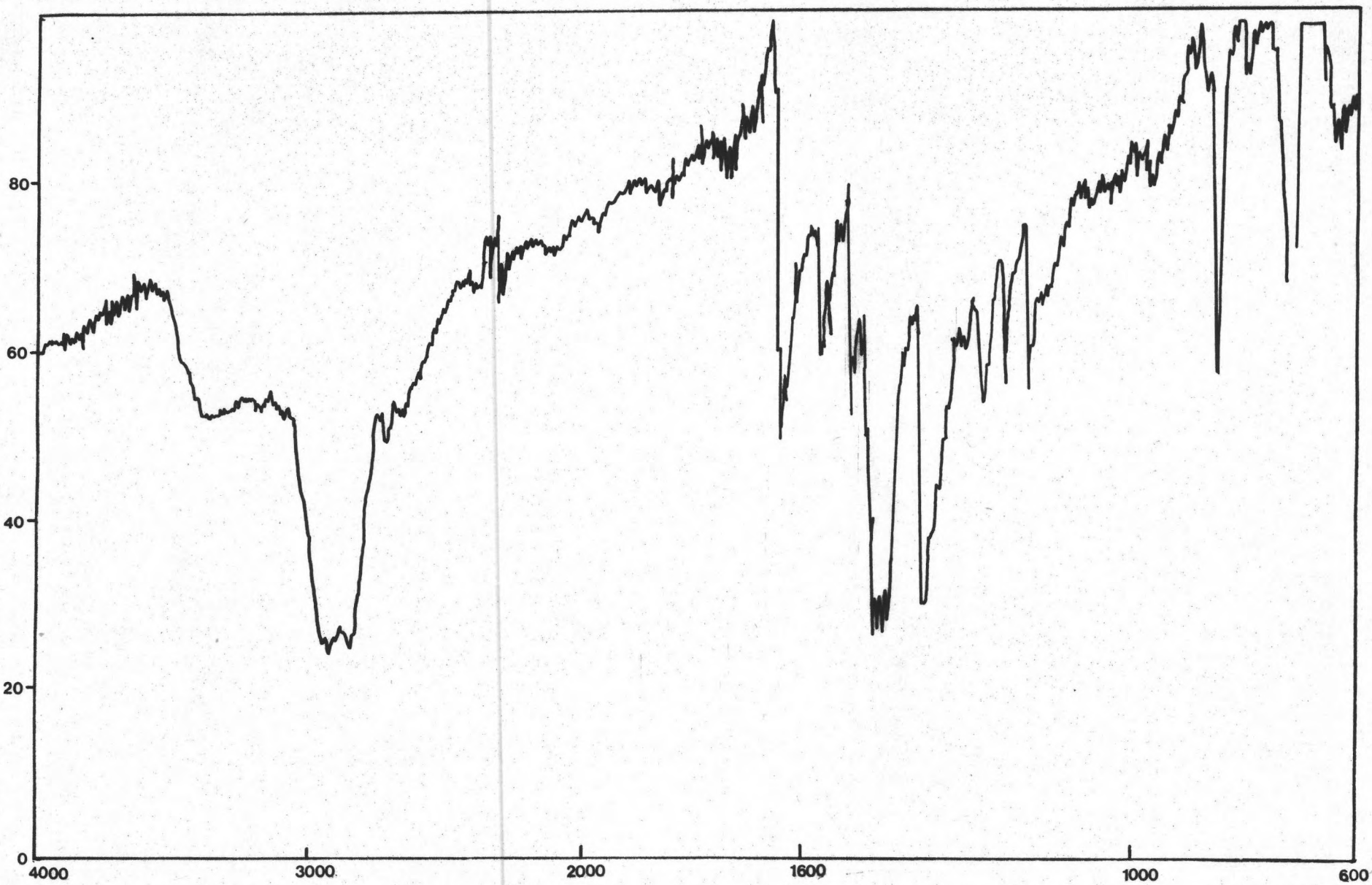

Figure 3.11 Infrared spectra of paraquat

Hydrogen Bonding

1. Bond Length Calculation

The most precise semi-empirical relation describing the decrease of stretching frequency vibrations in comparison to vibration of free OH was proposed by Bellamy and Owen (54). According to these authors the decrease of frequency (Δ) in cm^{-1} can be calculated from the Lennard-Jones 12-6 potential function:

$$\Delta = 50\left[\left(\frac{d}{R}\right)^{12} - \left(\frac{d}{R}\right)^{6}\right]$$

where

d = a value close to the sum of collision radii of atoms X and Y in the X-H---Y bond

R = hydrogen bond length

This formula was used for the calculation of hydrogen bond lengths in kaolinite, according to the structural scheme of interlayer bonding adapted from Giese and Datta (48) and presented in Figure 3.12. Wieckowski and Wiewiora (15) chose the value of d close to the collision radii of oxygen and found that the each total hydrogen bond length (the distance between the two oxygen atoms involved in hydrogen bonding) was shorter than the corresponding value obtained from X-ray diffraction methods. The differences were explained in terms of the nonlinearity of the hydrogen bonds.

It seem reasonable in this work, however, to make a rough estimate of the value of d by combining the x-ray results and the 12-6 potential function. Thus the values of the O---O distances were substituted into the Lennard-Jones potential function, using Δ values from the IR data, and the d values were found to be 2.79, 2.86 and 2.77 Å which are much closer to the Van der Waals radius of oxygen than to the collision

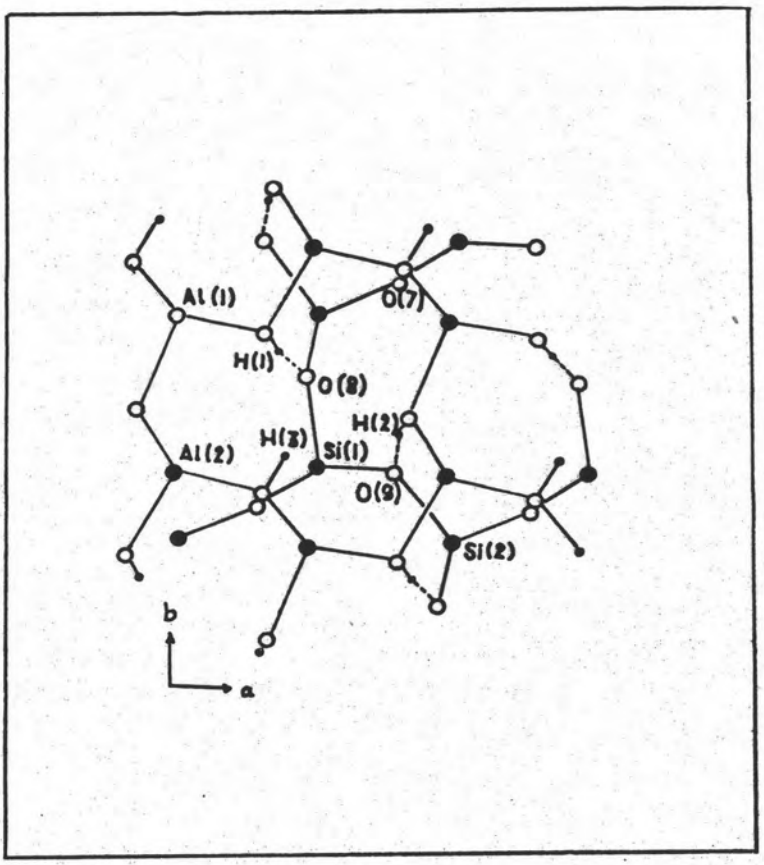

Figure 3.12 The projection of the two atomic planes in the octahedral and similarly in the tetrahedral sheets of the adjacent layers onto (001).after Giese and Datta (1973). The (O) are oxygens, the (●) are cations and the (●) are hydrogen ions, the (----) represents the possible hydrogen bonds.

radius. Therefore, the value of d will be taken to be the sum of the van der Waals radii of oxygen which is 2.8 Å(54).

By using computer technique four maximum absorption bands of Bang Rin kaolinite were found to be at 3617, 3652, 3667 and 3691 cm^{-1}. Taking 3742 cm^{-1} as the vibration frequency of 'free' OH group(15) and assuming that the band at 3617 cm^{-1} corresponds to OH groups which are not involved in interlayer bonding, the frequency shifts (Δ) of the remaining three bands are found to be 90, 75 and 51 cm^{-1}, respectively.

With the chosen d value, substitution into the 12-6 potential gives the total hydrogen bond lengths (R) tabulated in Table 3.8.

Normally, when the oxygen atoms of two 'molecules' are closer together than the sum of the van der Waals radii, the presence of hydrogen bond(s) is inferred. Results shown in Table 3.8 show that this is the case. And since the values of R are smaller than the corresponding, there is no need to consider the nonlinearity of the bonds.

On the contrary, the assumption of nonlinearity made by Wieckowski and Wiewiora(15) is unreasonable in terms of the fact that R should be taken as the distance between the two oxygen molecules along the direction of shortest approach and not as the sum of the O-H and H---O bonds.

2. Bond Energy Calculation

Results of computation of the bulk energy of the hydrogen bonds and of their components V_1, V_2 and V_3+V_4 are presented in Table 3.10.

From Table 3.10 the energy of the hydrogen bond V_1, V_2, V_3, V_4 and V decreases as the interlayer distance O-O increases.

In Table 3.11, the energies of hydrogen bonds in kaolinite calculated from the i.r. data are compared with the energy of hydrogen bonds given by various authors. The results agree with the other authors although the values of V_1, V_2, V_3, V_4 and V are slightly higher in this work.

In the previous work the bond energy of $O_{(3)}$-H---$O_{(7)}$ was 2.65 kJ/mol, and the bond was classified as a declining hydrogen bond. In this work all of the bond energies were attributed to the short bonds and were within limits of hydrogen bond energies as given by various authors (Table 3. 11).

Results presented in Tables 8-11 supply sufficient data to prove that the cohesion between the kaolinite layers may be considered as hydrogen bonding and that no coupling phenomena occurs between the hydroxyl groups.

The frequencies of the stretching vibrations of the three hydroxyls involved in the interlayer bonding are lower than those of the 'free' superficial hydroxyls in the external plane of the octahedral sheet and not involved in hydrogen bonding.

Frequency decrease is roughly on the order of 50-100 cm^{-1} (Table 3-8). The differences in these frequency shifts (from 3742 cm^{-1}) are reflected in the values of the total hydrogen bond energies and in the values of their components.

Table 3.8 Comparison of the hydrogen bond lengths and interlayer distances O-O in kaolinite.

Pairs of oxygen shown in Figure 3.11	Δ (cm^{-1}) frequency shift free OH-OH in hydrogen bond	Hydrogen bonds length R from I.R. data (Å)	Interlayer O-O distance from diffraction data after Giese and Patta (Å)
$O_{(2)}$---$O_{(9)}$	3742-3652 = 90	2.51	2.89
$O_{(1)}$---$O_{(8)}$	3742-3667 = 75	2.53	2.90
$O_{(3)}$---$O_{(7)}$	3742-3691 = 51	2.58	3.02

Table 3.9 Parameters and constants for hydrogen bond system of the type O-H-O

D_o (kJ/mol)	493.71
n (m^{-1})	9.18×10^{10}
n^* (m^{-1})	13.32×10^{10}
r_o (m)	0.97×10^{-10}
r_o^* (m)	0.97×10^{-10}
k_o (N/m)	7.76×10^{2}
k_o^* (N/m)	7.76×10^{2}
b (m^{-1})	4.80×10^{10}
m	1

Table 3.10 Values of the entire energy V of the hydrogen bonds, values of van der Waals repulsion V_3, and electrostatic attraction V_4.

Oxygen involved in hydrogen bonds	Interlayer distance O - O (Å)	Frequency of Vibration (cm^{-1})	V_1 kJ/mol	V_2 kJ/mol	$V_3 + V_4$ kJ/mol	V kJ/mol
$O_{(2)}\cdots O_{(9)}$	2.51	3652	39.50	-138	52.73	-45.76
$O_{(1)}\cdots O_{(8)}$	2.53	3667	29.62	-120	48.04	-42.34
$O_{(3)}\cdots O_{(7)}$	2.58	3691	17.28	-90	37.79	-34.93

Table 3.11 Comparison of the energies (in kJ/mol) of hydrogen bonds in kaolinite calculated from the i.r. data with those given by various authors.

This work	Tadeusz Wieckowski and Andrzej Wiewiora (1976)	Kecki (1975)	Novak (1974)	Coulson (1963)
$O_{(2)}-H\cdots O_{(9)}$ 45.76	19.63			
$O_{(1)}-H\cdots O_{(8)}$ 42.34	16.71	12.55-29.29	8.37-41.84	11.30-33.47
$O_{(3)}-H\cdots O_{(7)}$ 34.93	2.65			